

# ANALYTIC THEORY OF ABSOLUTE NEGATIVE MOBILITY IN A MICROFLUIDIC DEVICE\*

RALF EICHHORN, PETER REIMANN

Universität Bielefeld, Fakultät für Physik, 33615 Bielefeld, Germany

*(Received January 9, 2006)*

*Dedicated to Professor Peter Talkner on the occasion of his 60th birthday*

We theoretically discuss and analyze the design of a microfluidic device which has recently been demonstrated experimentally to exhibit the phenomenon of absolute negative mobility (*i.e.* net motion into the direction opposite to a net acting force) for non-interacting Brownian particles. Based on a model for the motion of a colloidal particle in a structured microfluidic system, that includes electroosmotic and electrophoretic effects as well as thermal fluctuations, we derive an analytic approximation for the average particle velocity, comparing very well with data of numerical simulations and experimental measurements.

PACS numbers: 85.85.+j, 05.40.-a, 05.60.-k, 82.70.Dd

## 1. Introduction

Peter Talkner continuously delivered outstanding contributions to the topics of stochastic modeling and escape rate theory since his early years [1–7], while microfluidics represents a more recent one among his manifold fields of interest [8,9]. To a large extent, our own steps in these two directions can be ultimately traced back to him and are combined here for the purpose of deriving an approximate analytical theory for the recently reported phenomenon of absolute negative mobility in a structured microfluidic device [10].

The second law of thermodynamics imposes strong restrictions on the possible response behavior of equilibrium systems to external perturbations. For instance, when applying a static force on a particle which is in equilibrium with its thermal environment (heat bath), the particle has to move

---

\* Presented at the XVIII Marian Smoluchowski Symposium on Statistical Physics, Zakopane, Poland, September 3–6, 2005.

in the direction of that force; any other behavior, such as a motion in the opposite direction, is ruled out, since it could be exploited to extract useful work from a single heat bath.

However, there are no such *a priori* restrictions for non-equilibrium systems. Accordingly, their response to external perturbations may be quite intriguing or even paradoxical. Indeed, for a thermally disequilibrated Brownian particle net transport in the direction *opposite* to the static external force independently of the sign of the force (so-called *absolute negative mobility* or, briefly, ANM) has been predicted theoretically in various idealized model systems [11–13], and has recently been demonstrated experimentally in a microfluidic device [10]. A related but different non-equilibrium phenomenon is the prominent ratchet effect [14], characterized by directed particle motion without systematic force.

In the present contribution, we discuss the theoretical challenges when stepping beyond the idealized model systems of Refs. [11–13] towards realistic experimental set-ups. For the design of such realistic set-ups, the findings from the idealized models serve as a valuable guide. In particular, one can identify the crucial ingredients for the occurrence of ANM, namely: thermal noise, causing diffusive motion of the particle, and force-dependent particle traps, typically realized by “dead-ends” or “corners” in a periodic two-dimensional potential landscape into which the particle is pressed by external forces [12, 13]. As a specific experimental system, we consider the set-up of [10], and derive a quantitative analytical theory that is in good agreement with numerical simulations and with the experimental measurements.

## 2. Experimental framework and the problem with the traps

A microfluidic device (“lab-on-a-chip”) naturally equips us with what we need for the experimental realization of ANM: Due to the smallness of the device thermal noise plays a considerable role. Colloidal particles or biological constituents (cells, organelles, *etc.*) of micrometer size which are suspended in low concentration in an aqueous buffer solution thus represent non-interacting Brownian particles. In an aqueous environment, such particles typically acquire surface charges so that non-equilibrium drivings as well as external forces on the particles can be readily imposed by electric fields. Moreover, a two-dimensional potential landscape can be built with topographical structures, using standard micro-structuring techniques such as soft lithography [16].

With this experimental framework in mind, the theoretical studies [12, 13] suggest several possibilities for periodically structured “micro-channels” with “dead-ends” or “corners” as particle traps that are known to supply ANM.

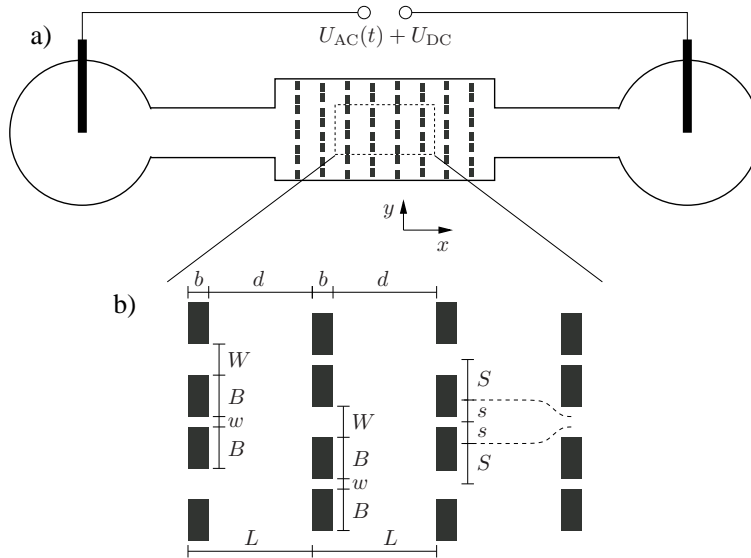


Fig. 1. (a) Schematic top view ( $x$ - $y$  plane, not to scale) of the experimental set-up reported in [10]: The microfluidic device consists of a microstructured central part connected to two inlet/outlet channels with fluid reservoirs at their ends. Via electrodes that are immersed into the reservoirs electric potential differences can be applied along the  $x$ -direction. The system is driven away from thermal equilibrium by a time-dependent signal  $U_{AC}(t)$  that jumps periodically between  $\pm U_0$  ( $U_0 > 0$ ) with period  $2\tau$ ; the static perturbation is realized by a static voltage  $U_{DC}$ . (b) Enlargement of the structured part of the microfluidic device: Rows of rectangular posts (“obstacles”) with alternately small and large gaps between the post are arranged periodically in  $x$ -direction such that the gaps are in line and again alternate between small and large. The microdevice is specified by the widths  $w$  and  $W$  of the small and large gaps, respectively, the size  $b \times B$  of the posts, the distance  $d$  between subsequent rows, and the particle radius  $r$ , where  $w < r < W$  is required. The spatial period in  $x$ -direction is  $2L = 2(b + d)$ . The dashed lines illustrate the border of the deterministic attraction basin of a small gap (a “trap”, see Sec. 4 of the main text and Fig. 2 for a detailed explanation); its location is characterized by the quantities  $s$  and  $S$  with  $2(s + S) = w + W + 2B$ .

However, as it turns out, these structures are not suitable to generate ANM in a microfluidic device for the following reason. Since the buffer solution is in good approximation an ideal conductor, whereas the structured material is an insulator, the electric field at the border between fluid and microstructure has no component perpendicular to the walls of the microstructure. As a consequence, “dead-ends” or “corners” do not act as particle traps; the field lines just follow the outline of the structure instead of pressing the charged particle into the “dead-ends” or “corners”. Moreover, it is also not

possible to generate traps with static electric fields in the field region away from the walls (which is free of space-charges) due to Earnshaw's Theorem [17]; a trapping region would have an electric field very similar to that of a space-charge, *i.e.* it would be a sink (or source) of electric field lines. Similarly, a force field that is imposed on the particle by a streaming fluid (*e.g.* electroosmotically or pressure driven) is not suitable to generate particle traps for the same reasons: the flow can not penetrate through the structured material, and there are no fluid sinks (or sources) within the device.

The solution to this problem is shown in Fig. 1. Instead of “dead-ends” or “corners”, the traps are realized by tiny gaps in the microstructure, that are smaller than the size of the colloidal particles, so that the electric (or streaming) field lines can pass through them but the particle cannot. Indeed, this structure has been used for the experimental realization of ANM in [10]; a sketch of the complete experimental set-up is shown in Fig. 1. As a side remark we mention that a very similar microstructure has been considered theoretically in [18], however in a different physical context.

### 3. Model

We model the motion of a colloidal particle (“bead”) in the microstructure with coordinates  $\vec{r}=(x, y, z)$  by the stochastic dynamics [4, 19]

$$\gamma\dot{\vec{r}} = F(\vec{r}) + q\vec{E}_*(\vec{r})\frac{U_{\text{AC}}(t) + U_{\text{DC}}}{U_*} + \vec{\xi}(t), \quad (1)$$

where  $\vec{r}=\vec{r}(t)$ , inertia effects are neglected (overdamped dynamics), and  $\gamma$  denotes the viscous friction coefficient [11–14]. The force field  $\vec{F}(\vec{r})$  derives from an effective hard-wall potential of the microstructure (incorporating the finite particle radius), while  $q\vec{E}_*(\vec{r})$  is the effective force on the bead generated by a constant reference voltage  $U_* = 1\text{ V}$  applied to the electrodes in Fig. 1(a). Thermal fluctuations are modeled as usual [4, 14] by  $\vec{\xi}(t) = (\xi_x(t), \xi_y(t), \xi_z(t))$ , where  $\xi_\alpha(t)$ ,  $\alpha \in \{x, y, z\}$  are independent, unbiased Gaussian noise sources, satisfying the fluctuation dissipation relation [2]  $\langle \xi_\alpha(t) \xi_\alpha(t') \rangle = 2\gamma kT\delta(t - t')$ , with Boltzmann's constant  $k$  and room temperature  $T \approx 290\text{ K}$ .

In Eq. (1)  $q$  quantifies the effective force on the charged particle due to the applied electric field, which contains two dominating electrokinetic effects: The force on the charged bead due to the applied electric field (electrophoresis), and the force on the particle due to the streaming buffer solution, being set in motion by electroosmosis [15]. That also the latter effect can be described by a force field proportional to the electric field under quite general conditions can be shown by exploiting a remarkable similitude

between electrophoresis and electroosmosis recently unraveled in [20]. The coupling  $q$  to the electric field thus represents an effective charge only in a very loose sense [21]. Much like the effective coupling  $\gamma$  to the thermal environment, it depends in a very complex way on the geometry and the chemical surface properties of microstructure and bead, as well as on the electrohydrodynamic buffer properties. Therefore, to quantitatively adapt the model (1) to a given experimental situation, the model parameters  $q$  and  $\gamma$  have to be determined experimentally, *e.g.* by measuring the diffusion coefficient

$$D_0 = \frac{kT}{\gamma}, \quad (2)$$

and the (voltage-dependent) free velocity

$$v_0 = \mu_0 U, \quad (3)$$

of the particle with  $\mu_0 = (q/\gamma) \vec{E}_*(\vec{r})/U_*$  within an unstructured region of the device [10, 19]. In the following, we adopt the sign-convention for  $q$  such that a positive voltage applied to the electrodes in Fig. 1 generates a positive force on the particle along the  $x$ -axis, and analogously for a negative voltage.

To determine the electric field  $\vec{E}_*(\vec{r})$  in (1), the Laplace equation is solved within the microstructured region, where its periodicity in  $x$ - and  $y$ -direction (see Fig. 1) is taken into account with the choice of the boundary conditions: Along the  $y$ -axis, periodic boundary conditions are used; along the  $x$ -axis, a preset potential difference over several spatial periods is imposed and the resulting “central unit cell” periodically continued. Moreover, assuming that the buffer solution is a perfect (electric) conductor and the microstructure is a perfect insulator, Neumann boundary conditions are adopted at the borders between microstructure and buffer. Typical results for the resulting force field  $q\vec{E}_*(\vec{r})$  in (1) are illustrated by the grey arrows in Fig. 2.

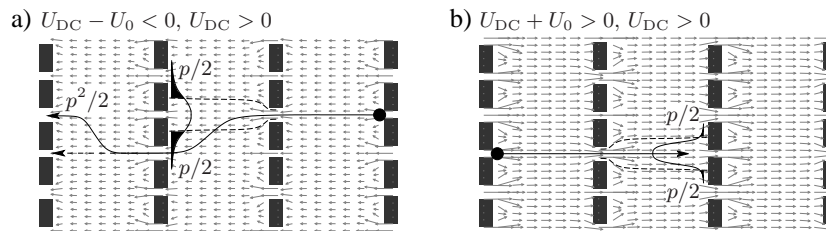


Fig. 2. Schematic illustration of the particle motion in the microstructure from Fig. 1 for  $U_{\text{DC}} > 0$ ,  $U_{\text{DC}} < U_0$ . The probabilities for several traveling routes are indicated. For more details see main text, Sec. 4. (a) Motion during a half-period of duration  $\tau$  with total voltage  $U_{\text{DC}} - U_0 < 0$ . (b) Motion during a subsequent half-period of duration  $\tau$  with total voltage  $U_{\text{DC}} + U_0 > 0$ .

#### 4. Physical mechanism for ANM

Based on the model (1) we can now discuss qualitatively the dynamical behavior of the particle in the microfluidic set-up of Fig. 1 [10, 19]. Specifically, we are interested in the response of the non-equilibrium system in Fig. 1(a) when it is perturbed by a static voltage  $U_{\text{DC}}$ . Since the non-equilibrium situation is established by a time-dependent voltage  $U_{\text{AC}}(t)$  that jumps periodically between  $\pm U_0$  ( $U_0 > 0$ ) with period  $2\tau$ , the total applied voltage  $U_{\text{AC}}(t) + U_{\text{DC}}$  periodically adopts the values  $U_{\text{DC}} \pm U_0$ . For symmetry reasons it is sufficient to consider the case  $U_{\text{DC}} > 0$ ; moreover, we restrict ourselves to the most interesting response regime with  $U_{\text{DC}} < U_0$ . In addition to the thermal fluctuations, the particle motion in the microstructure is thus subjected to a deterministic force due to the applied electric field, which switches between the two states illustrated with Fig. 2(a) and (b) (the arrows indicate direction and magnitude of the force field).

Fig. 2(a) sketches the motion of a bead while the total voltage  $U_{\text{DC}} - U_0 < 0$  is acting. Though the field is spatially inhomogeneous, the  $x$ -component of the force always points in the same (negative) direction as the total voltage. As already mentioned, the small gaps between the posts act as deterministic “traps”, because the field lines can pass through them, but the bead can not. For one of them, the border of the attraction basin is indicated by the dashed lines in Fig. 2(a). Once the bead is trapped by a small gap, the probability to escape by thermal noise is negligible. In order to avoid such a trap, the particle has to pass by thermal diffusion over the dashed basin-boundary during its traveling time from one row of posts to the next. The probability of doing so is indicated in Fig. 2(a) by the filled tails of the distribution of an ensemble of beads which started out in the adjacent large gap to the right. Once the particle has succeeded in avoiding the trap, it is either caught by the next trap (dashed arrow in Fig. 2(a)) to the left or it again succeeds in avoiding it (solid arrow in Fig. 2(a)), and so on. If the half-period  $\tau$  with constant total voltage  $U_{\text{DC}} - U_0 < 0$  is sufficiently long, the particle is finally caught by some trap and remains there for the rest of the time  $\tau$ . Subsequently, the voltage changes its sign and takes the constant value  $U_{\text{DC}} + U_0 > 0$  for the next half-period  $\tau$ , as illustrated by Fig. 2(b). Assuming  $U_{\text{DC}} > 0$ , the total voltage and hence the forces are larger in modulus and of opposite sign compared to Fig. 2(a). Accordingly, the traveling time from one row of posts to the next is shorter and the diffusive dispersion narrower. Likewise, the probability to avoid a trap is smaller in Fig. 2(b) than in Fig. 2(a) and hence the average traveling distance smaller. Finally, the particle is again caught by some trap, remains there for the rest of the second half-period  $\tau$ , and the cycle restarts with Fig. 2(a).

The overall result is a net motion in the negative  $x$ -direction, *i.e.* opposite to the assumed positive static DC-voltage  $U_{\text{DC}} > 0$ . Obviously, things are analogous for  $U_{\text{DC}} < 0$ .

In other words, we expect to observe ANM in the set-up of Fig. 1 generically, provided that the driving period  $2\tau$  is large enough such that the particle can at least travel one spatial period from its initial small gap through a large gap to the next small gap during each half-period  $\tau$ . This prediction is nicely confirmed by the response curves in Fig. 3, showing the distinct and unambiguous signature of ANM: a negative slope symmetrically around the origin. (The detailed discussion of the sign change of  $v$  for large static perturbations  $U_{\text{DC}}$  in Fig. 3 is beyond the scope of our present paper.)

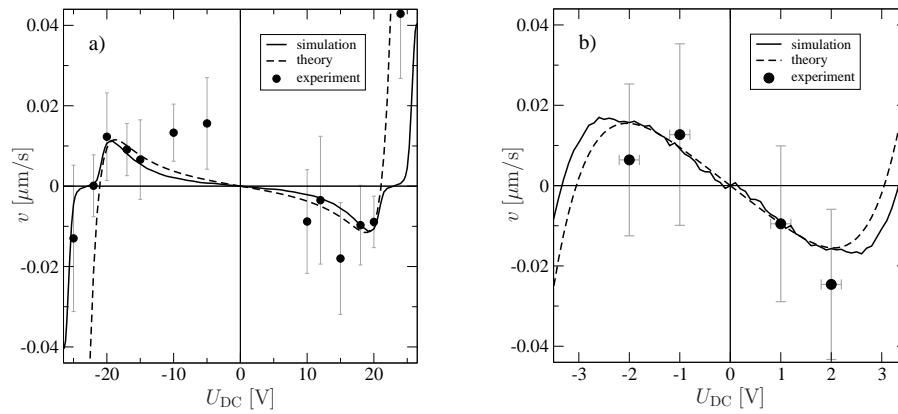


Fig. 3. Absolute negative mobility for two different species of Brownian particles in the microfluidic device from Fig. 1 with  $w = 1.7 \mu\text{m}$ ,  $W = 3.1 \mu\text{m}$ ,  $b = 3.1 \mu\text{m}$ ,  $B = 6.1 \mu\text{m}$ , and  $d = 22.5 \mu\text{m}$ . Solid curves: Response characteristics obtained by numerical simulations of (1). Dashed curves: Theoretical approximation of the average particle velocity according to (5)–(10a). Dots with error bars: Experimentally measured average velocity from [10, 19]. (a) Colloidal particles with  $r = 1.0 \mu\text{m}$ ,  $\mu_0 = 0.23 \mu\text{m}/(\text{Vs})$ ,  $D_0 = 0.063 \mu\text{m}^2/\text{s}$  [10, 19] in the presence of a driving  $U_{\text{AC}}(t)$  with amplitude  $U_0 = 30 \text{V}$  and switching time  $\tau = 25 \text{s}$ . (b) Colloidal particles with  $r = 0.95 \mu\text{m}$ ,  $\mu_0 = 0.28 \mu\text{m}/(\text{Vs})$ ,  $D_0 = 0.131 \mu\text{m}^2/\text{s}$  [19] in the presence of a driving  $U_{\text{AC}}(t)$  with amplitude  $U_0 = 6 \text{V}$  and switching time  $\tau = 70 \text{s}$ . For more details about the experimental determination of  $\mu_0$  and  $D_0$  see [19].

## 5. Average particle velocity

In order to quantify the above qualitative insights, we now derive an analytical approximation for the average particle velocity in  $x$ -direction,

$$v := \lim_{t \rightarrow \infty} \frac{x(t)}{t}. \quad (4)$$

The first step consists in a similar line of reasoning as in [12]: Based on the observation that the particle starts out from a small gap at the beginning of each half-period of the driving (see Fig. 2 and discussion in the preceding section), (4) can be rewritten as

$$v = \frac{\Delta x(\tau, U_0 + U_{\text{DC}}) - \Delta x(\tau, U_0 - U_{\text{DC}})}{2\tau}, \quad (5)$$

where  $\Delta x(\tau, U)$  is the average traveling distance of the particle along the  $x$ -direction within a half-period  $\tau$  when a constant voltage  $U$  is applied. In (5), we exploited that  $\Delta x(\tau, -U) = -\Delta x(\tau, U)$  due to the symmetry properties of our system (see Fig. 1). The average traveling distance  $\Delta x(\tau, U)$  results from the above described behavior of the bead that during each half-period  $\tau$  it first travels the “basic” distance of approximately  $2L$  from its initial small gap to the first trap, and that it then can proceed further for an additional distance  $L$  whenever it succeeded in avoiding a trap, until it is finally caught in some trap (see also Fig. 2). Assuming that the probability  $p$  for avoiding a trap is approximately the same for all traps independently of the pre-history of the particle motion and adopting a maximal traveling distance (avoiding all traps) of the form  $L(2 + N)$  (with  $N \in \mathbb{N}$ ), the average traveling distance  $\Delta x(\tau, U)$  follows as  $L(2 + p + p^2 + \dots + p^N)$  (cf. Fig. 2(a)). With the free particle velocity  $v_0$  from (3) we obtain  $L(2 + N) = \mu_0 U \tau$  and hence

$$\Delta x(\tau, U) = L \left( 1 + \frac{1 - [p(U)]^{\frac{\mu_0 \tau U}{L} - 1}}{1 - p(U)} \right). \quad (6)$$

This expression remains a reasonable interpolation even if  $\mu_0 U \tau$  is not precisely of the form  $L(2 + N)$  with  $N \in \mathbb{N}$ .

The probability  $p$  for avoiding a trap is identical to the probability that the particle diffuses beyond the attraction basin of the trap during its motion in  $x$ -direction from the preceding large gap towards that trap (see Fig. 2). To calculate  $p$  we first observe that the force field between two row of posts is practically homogeneous except for small regions in the vicinity of the gaps, where the field either “extends” from its restriction to the gap, or else is “squeezed” into the gap, see Fig. 2. The sizes of these regions in  $y$ -direction are determined by the borders of the deterministic attraction basins of the gaps; we denote them by  $s$  and  $S$  for the small and the large gaps, respectively (see Fig. 1(b)). Their extensions in  $x$ -direction can be estimated as  $s - w/2$  at the small and  $S - W/2$  at the large gaps, so that the homogeneous field region extends over approximately  $d_{\text{D}} = d - s - S + (W + w)/2$  in  $x$ -direction, where  $d > s + S - (W + w)/2$  is tacitly assumed. Within the inhomogeneous field regions  $s$  and  $S$ , the  $y$ -component of the bead motion is dominated by the deterministic force field, whereas it is

dominated by diffusion in the homogeneous field region  $d_D$  between two rows of posts. Hence, an ensemble of particles starting in a large gap is first “broadened” deterministically in  $y$ -direction by a factor  $\alpha = 2S/W$  (see Fig. 1(b)), and then freely diffuses with the diffusion coefficient  $D_0$  from (2) in  $y$ -direction while traveling with constant velocity  $v_0$  according to (3) over a distance  $d_D$  in  $x$ -direction, until it is split within the inhomogeneous field region into a part that is trapped in the small gap and two parts that avoid the trap and instead are attracted to one of the two adjacent large gaps in the same row of posts (see also Fig. 2). Assuming a starting ensemble of particles that is uniformly distributed over the “accessible” width  $W - 2r$  of the large gap ( $r$  is the particle radius), the  $y$ -dependent particle density just before that splitting reads

$$\begin{aligned} \rho_U(y) &= \frac{1}{\alpha(W - 2r)} \int_{-\alpha(W-2r)/2}^{\alpha(W-2r)/2} dy_0 \frac{e^{-(y-y_0)^2/[4D_0d_D/(\mu_0U)]}}{\sqrt{4\pi D_0d_D/(\mu_0U)}} \\ &= \frac{1}{2\alpha(W - 2r)} \left( \operatorname{erf} \left[ \frac{(y + \frac{\alpha}{2}(W - 2r))\sqrt{\mu_0U}}{\sqrt{4D_0(d - B)}} \right] \right. \\ &\quad \left. - \operatorname{erf} \left[ \frac{(y - \frac{\alpha}{2}(W - 2r))\sqrt{\mu_0U}}{\sqrt{4D_0(d - B)}} \right] \right), \end{aligned} \tag{7}$$

where the origin of the  $y$ -axis is located at the center of the (small) gap,  $\operatorname{erf}(z) := 2\pi^{-1/2} \int_0^z dt e^{-t^2}$ , and where  $d_D = d - s - S + (W + w)/2 = d - B$  (cf. Fig. 1(b)) has been used. The assumption of a uniform initial distribution in the large gaps approximately takes into account the diffusion of the particle in  $y$ -direction on its way towards the large gap. Finally, the probability  $p$  for avoiding the trap is given as

$$p(U) = 2 \int_s^\infty dy \rho_U(y). \tag{8}$$

To estimate the size of the deterministic attraction basins of the traps, *i.e.* to approximate the quantities  $s$  and  $S$  (see Fig. 1(b)), we recall that the force field is proportional to  $\vec{E}(\vec{r})$ , cf. Eq. (1), and that the electric field has the “incompressibility” property  $\vec{\nabla} \cdot \vec{E}(\vec{r}) = 0$ . Assuming that the (mean) electric field amplitudes in the small and large gaps are approximately the same, we can thus read off from Fig. 1(b) that the “broadening” factor  $\alpha$  fulfills the relation  $\alpha = 2S/W = 2s/w = 2(S + s)/(W + w)$ . It readily follows that

$$\alpha = \frac{2B}{W + w} + 1, \quad (9)$$

and

$$s = \frac{Bw}{W + w} + \frac{w}{2}, \quad (10a)$$

$$S = \frac{BW}{W + w} + \frac{W}{2}. \quad (10b)$$

In summary, our approximation of the average particle velocity (4) is given by (5), where the average traveling distance  $\Delta x(\tau, U)$  is obtained from (6), the probability  $p(U)$  for avoiding a trap from (7), (8), and the geometrical quantities  $\alpha$  and  $s$  from (9) and (10a), respectively. The resulting theoretical curves in Fig. 3 are in good agreement with the numerical findings, in particular in view of the various approximations in the derivation of (6)–(10a).

## 6. Conclusion

In this contribution, we discussed the non-equilibrium phenomenon of absolute negative mobility (ANM) from the viewpoint of an experimental realization. In particular, we focused on the difficulties and possibilities one encounters when realizing the crucial ingredients for ANM — diffusion and particle traps, identified in previous works on simplified model systems [11–13] — with a microfluidic device [10], see Fig. 1. Starting from the stochastic differential equations (1) as a theoretical model for this microfluidic set-up [19], we derived the analytic approximation (5)–(10a) for the average particle velocity (4) in response to a static external perturbation. The model (1) covers the microstructured potential landscape, thermal fluctuations, and, due to their similitude [20], electrophoretic and electroosmotic forces on the particle, which are the two most important electrokinetic effects in our case. Once the unknown effective coupling  $\gamma$  to the thermal heat bath and the effective coupling  $q$  to the electric field (see Eq. (1) and subsequent discussion) have been experimentally determined, the model (1) can be used to make quantitative predictions for the microfluidic ANM-experiment. Its reliability has been established in [10, 19] by direct comparison with several experimental measurements; for the sake of completeness those experimental results are also reproduced in Fig. 3, showing excellent agreement with the theoretical model (1).

We thank our experimental partners J. Regtmeier, T.T. Duong, D. Anselmetti and A. Ros for admitting the reproduction of their experimental data in Fig. 3. This work has been supported by the Deutsche Forschungsgemeinschaft under SFB613, and by the ESF program STOCHDYN.

## REFERENCES

- [1] H. Grabert, P. Talkner, P. Hänggi, *Z. Phys.* **B26**, 389 (1977).
- [2] H. Grabert, P. Hänggi, P. Talkner, *J. Stat. Phys.* **22**, 537 (1980).
- [3] P. Talkner, *Z. Phys.* **B68**, 201 (1987).
- [4] P. Hänggi, P. Talkner, M. Borkovec, *Rev. Mod. Phys.* **62**, 251 (1990).
- [5] P. Talkner, *Chem. Phys.* **180**, 199 (1994).
- [6] P. Talkner, *New J. Phys.* **1**, 4 (1999).
- [7] P. Talkner, L. Machura, M. Schindler, P. Hänggi, J. Luczka, *New J. Phys.* **7**, 14 (2005).
- [8] Z. Guttenberg, A. Rathgeber, S. Keller, J. Rädler, A. Wixforth, M. Kostur, M. Schindler, P. Talkner, *Phys. Rev.* **E70**, 056311 (2004).
- [9] M. Kostur, M. Schindler, P. Talkner, P. Hänggi, *Phys. Rev. Lett.* **96**, 014502 (2006).
- [10] A. Ros, R. Eichhorn, J. Regtmeier, T.T. Duong, P. Reimann, D. Anselmetti, *Nature* **436**, 928 (2005).
- [11] P. Reimann, R. Kawai, C. Van den Broeck, P. Hänggi, *Europhys. Lett.* **45**, 545 (1999); B. Cleuren, C. Van den Broeck, *Phys. Rev.* **E65**, 030101(R) (2002); B. Jiménez de Cisneros, P. Reimann, J.M.R. Parrondo, *Europhys. Lett.* **64**, 599 (2003); R. Eichhorn, P. Reimann, *Acta Phys. Pol. B* **35**, 1407 (2004); R. Eichhorn, P. Reimann, B. Cleuren, C. Van den Broeck, *Chaos* **15**, 026113 (2005).
- [12] R. Eichhorn, P. Reimann, P. Hänggi, *Phys. Rev. Lett.* **88**, 190601 (2002); *Phys. Rev.* **E66**, 066132 (2002).
- [13] R. Eichhorn, P. Reimann, P. Hänggi, *Physica A* **325**, 101 (2003); B. Cleuren, C. Van den Broeck, *Phys. Rev.* **E67**, 055101(R) (2003).
- [14] P. Reimann, *Phys. Rep.* **361**, 57 (2002); J. Klafter, M. Urbakh (special Issue guest editors), *J. Phys.: Condens. Matter* **17**, S3661–4024 (2005).
- [15] G.E. Karniadakis, A. Beskok, *Microflows–Fundamentals and Simulation*, Springer, New York 2002.
- [16] S.R. Quake, A. Scherer, *Science* **290**, 1536 (2000).
- [17] See, for instance, the free online encyclopedia Wikipedia:  
[http://en.wikipedia.org/wiki/Earnshaw%27s\\_theorem](http://en.wikipedia.org/wiki/Earnshaw%27s_theorem).
- [18] M.G. Gauthier, G.W. Slater, *Electrophoresis* **24**, 441 (2003).
- [19] J. Regtmeier, R. Eichhorn, T.T. Duong, P. Reimann, D. Anselmetti, A. Ros, Particle sorting by absolute negative mobility in a microfluidic device, submitted for publication.
- [20] E.B. Cummings, S.K. Griffiths, R.H. Nilson, P.H. Paul, *Anal. Chem.* **72**, 2526 (2000).
- [21] D. Long, J.-L. Viovy, A. Ajdari, *Phys. Rev. Lett.* **76**, 3858 (1996).